Computational fluid dynamics investigation into flow behavior and acoustic mechanisms at the trailing edge of an airfoil

JACKSON, Beren and DAKKA, Sam <http://orcid.org/0000-0001-9225-761X>

CFD Investigation into Flow Behavior and Acoustic Mechanisms at the Trailing Edge of an Airfoil

Beren R. Jackson and Sam M. Dakka
Department of Engineering & Math, Sheffield Hallam University, Sheffield S1 1WB United Kingdom
Sam.dakka@gmx.com

Abstract

Airfoil self-noise or trailing edge noise and shear noise was investigated computationally for a NACA0012 airfoil section, focusing on noise mechanisms at the trailing edge to identify and understand sources of noise production using ANSYS Fluent. A two-dimensional computational fluid dynamics simulation has been performed for 0°, 8° and 16° airfoil angle of attack capturing surface pressure contours, contours of turbulent intensity, contours of surface acoustic power level, vorticity magnitude levels across the airfoil profile, and x and y directional self and shear noise sources across the airfoil profile. The results, indicate that pressure gradients at the upper surface do increase as the angle of attack increase which is a measure of vortices near the surface of the trailing edge associated with turbulence cease as the boundary layer begins to separate. Comparison of the turbulent intensity contours with surface acoustic power level contours demonstrated direct correlation between the energy contributed by turbulent structures (i.e. vortices), and the level of noise measured at the surface, and within the boundary layer of the airfoil. As angle of attack is increased both x and y sources have the same trends, however, y sources (perpendicular to the free-stream flow) appear to have a bigger impact as angle of attack is increased. Furthermore, as the angle of attack increased, shear noise contributes less and less energy further downstream of the airfoil, and becomes dominated by noise energy from vortical structures within turbulence. The two-dimensional computational fluid dynamics simulation revealed pressure, turbulent intensity and surface acoustic power contours, that further corroborated the previously tested noise observations phenomena at the trailing edge of the airfoil.

Keywords: airfoil self-generated noise, trailing edge noise, turbulent intensity, surface acoustic power level, shear noise.

1. Introduction

Stringent regulations on noise radiated by aircraft engines is getting tighter, this is due to forecast of future explosive growth in air transport that requires special attention in reducing noise emissions especially during landing approaches in airport neighboring communities. Therefore, knowledge of noise sources and mechanisms of noise production at the trailing edge of an airfoil is getting high priority in order to address and mitigate aircraft noise emissions. Furthermore, addressing the noise productions has wider implications on design of wind turbine blades, turbomachinery, ship hulls and airfoil design.

A review of self-generated noise mechanisms associated with subsonic flow surrounding an airfoil was defined by Brookes et al. [1]. Five airfoil self-generated noise mechanisms producing noise were described. At high Reynolds numbers, turbulent boundary layer is developed over most of the airfoil and broadband noise is generated as turbulence passes the trailing edge. At low Reynolds numbers laminar boundary develops at most of the airfoil, due to laminar boundary layer instabilities which cause vortex shedding and noise associated with the trailing edge. At non-zero angle of attack flow separation at the trailing edge on the upper surface and noise is generated due to turbulence shed vorticities. At higher angle of attack, large separation of the flow is encountered and the airfoil experience deep stall, in this regime low frequency noise is generated. Another source of radiated noise is vortex shedding in the wake of blunt trailing edge. The remaining noise sources are radiated due to development of airfoil tip vortices from turbulent flow. It is worth noting that boundary layer separation will generate several tonal peaks that are superimposed on the broadband noise, these are perhaps due to vortex shedding associated with the airfoil trailing edge.

An airfoil self-noise or Trailing edge-TE noise is defined when noise is generated due to vortical disturbances which are transformed into acoustical ones once they are convected downstream of the trailing edge. Roger and Moreau [2] had noted that attached or separated turbulent boundary layer at the trailing edge generates broadband noise, however whistles are generated due to laminar boundary disturbances. The self-noise production was addressed by Roger and Moreau [3] as a balance of forces encountered during the development of vortices traveled downstream due to pressure gradients and induced centrifugal forces. The geometrical singularity at the trailing edge cause further amplification of the radiated noise downstream as the flow maintain its adjustment through rapid reorganization of the vortical structures.

Two streams of ideas gained wide acceptance from the scientific noise communities, in relation to analytical analysis of self-noise generation. The first developed by Ffowcs Williams and Hall [4]. Where the noise radiated by the vortical disturbances of the boundary layer downstream of the trailing edge is related to the vortical velocity at the trailing edge. Amiet [5] and Howe [6] introduced the second approach which relates the far field acoustic signature statistics to the aerodynamic wall pressures statistics at some point upstream of the trailing edge. Based on this methodology the surface pressure is utilized as an equivalent acoustic source, though sound is generated due to the velocity field. An experimental verification for the second approach was accomplished by Brooks et al. [7] and Roger and Moreau [3] and was carried out successfully by Brooks and Hodgson [8].

2. Experimental data

The experimental apparatus of the NACA 0012 airfoil including the embedded microphone locations as a function of the chord length and analysis of the acoustic data were described and reported by the authors Jackson and Dakka [9]. To summarize the experimental findings for the energy/frequency spectra, towards the trailing edge the overall noise seen to be reduced and a reduction of the pressure can be observed. It appears that at the trailing edge, for smaller frequencies, the energy is *relatively* lower initially (than towards the leading edge), whereas past a certain point, noise energy towards the trailing edge is lost at a faster rate than at the leading edge. In general, for a laminar boundary layer they also appear to decrease in magnitude with angle of attack, whereas under a turbulent boundary layer the Strouhal numbers reported increase in magnitude with angle of attack.

It is interesting to note that the first four peak frequencies reported by Jackson and Dakka [9] do not deviate significantly between measurements at each angle of attack increase. The first, fifth

and ‘knee’ frequencies are not related harmonically, and so must be related to the behavior of the flow itself, or due to shear interactions between the flow and the airfoil surface. Based on frequency spectra in the range of around 1-10kHz, the steepening of the slope with increase in angle of attack was observed at microphone 1, and also the decay of the slopes of microphones 5 and 10 (see table 1 for chord locations). These observations could also be related to the steepening and magnitude of the adverse pressure gradient, and would suggest that for a given point, for different angles of attack, vortices are at different stages of development.

Another interesting observation based on the measured data is the fact that the sound pressure level stark behavior within the 3-10 kHz region and the 1-3 kHz region. The sound pressure level at microphone 10 appears to decay sooner as compared to microphone 5 as the angle of attack increase but still significantly higher than microphone 1, while for 1-3kHz SPL for microphone 10 is higher than microphone 5. This would suggest that there is in fact a higher amount of turbulent energy at microphone 5 in the region of about 3-10kHz, than there is at microphone 10, for lower angles of attack. Between 1-3kHz, it was suggested that the frequency spectra show a measure of the far-field noise energy; microphone 1 measures less energy in this portion because the boundary layer is still relatively small, effectively it may be measuring the free-stream flow energy outside of the boundary layer, whereas microphone 5 and 10 are actually measuring energy *within* the boundary layer, which has grown to a sufficient size at this point, and where microphone 5 detects the turbulent energy slightly closer to the outer edge of the boundary layer than does microphone 10, which measures a higher turbulent energy. Looking at the contours of turbulent intensity from the CFD simulation in figure 7, this visualization becomes clearer, and explains why microphone 10 measures higher energy than microphone 5, as angle of attack is increased, in the 1- 3kHz band.

On the other hand, between 3-10kHz, a phenomenon which would explain the differences in slope at microphones 5 and 10 is separation stall noise; as angle of attack is increased, the boundary layer at microphone 10 has a much higher affinity to separate (higher local Reynolds number) than microphone 5 (and microphone 1), therefore within the near-field region there is less energy due to small-scale vortical formations than there is at microphone 5, and effectively the only noise energy being measured is due to the back-draft of wake flow, which would also explain why the slope of microphone 10 becomes closer to microphone 5 as angle of attack is increased, since microphone 5 is also beginning to detect noise mechanisms due to wake flow. This theory was further supported, Jackson and Dakka [9], by the calculations of boundary layer thickness, skin friction and wall shear stress, which show that viscous forces do in fact reduce with location along the trailing edge.

3. **CFD Analysis:**

A two-dimensional computational fluid dynamics simulation has been performed for 0°, 8° and 16° angle of attack. The methodology and results are presented consequently.

3.1 Methodology

Initially a mesh, Figure 1 and 2, was generated for the NACA 0012 geometry with conditions similar to those tested in the physical acoustic wind tunnel testing [9]. This 2-D mesh domain involved an enclosure of around 5m x 4m, with a domed inlet. Sufficient space was left between the inlet and NACA 0012 airfoil (of chord 0.297m), and also between the trailing edge and the fluid outlet, in order to accurately capture free-stream flow, i.e. no intrinsic pressure sources could affect the external flow and thus the flow around the airfoil was accurately captured. The domed inlet allowed the inlet velocity components to be changed, thus allowing the same effect of rotating the airfoil and hence its angle of attack could be changed. Three simulations were

performed for 0°, 8° and 16°.

The generated mesh was of a very high quality, necessary for representative propagation of flow (essentially numerical calculations) between mesh cells (elements). There were 220472 elements, the smallest of which being at the surface and in high activity regions around the airfoil (such as the boundary layer and wake). Figure 3 shows the element metric graphs of orthogonal quality (a measure of quality for the incident quadrilateral cell mesh) and skewness (a measure of how stretched a mesh cell is).The graphs show how the majority of mesh elements are of extremely high quality and are minimally skewed. Table 2 gives values for the minimum, maximum and average of these element metrics (values range from between 0 to 1). The airfoil surface was given the characteristics of the same material used for the physical model, acrylonitrile butadiene styrene (ABS), and boundary conditions represented the characteristics of air at room temperature and with the same parameters as at sea level, the same environment in which the physical acoustic testing was done. The numerical solution method used was the 2-equation, transient based SST (shear stress transport) k-ω model, with a broadband noise, acoustics model solver. Other than solving for conservation of mass, momentum and energy, the parameters 'k' and 'ω' are the main functions calculated in this solver method, k being turbulent kinetic energy and ω being the specific dissipation rate of the turbulence, Bardina, Huang and Coakley [10]. The 'Shear Stress Transport' (SST) is an added factor in the model, developed by F.R. Menter [11], which increases accuracy for near wall treatment of the flow by considering effects of shear stress. The model is widely used for predicting aerodynamic flows with strong adverse pressure gradients and boundary layer separation, Menter, Kuntz and Langtry [11], and thus is sufficient for the current simulation.

In order for the solver to accurately predict the velocity of flow near to the airfoil surface, a value known as y+ has to be within a certain value. This parameter is a non- dimensional wall distance which is defined as follows $y^+ \equiv \frac{u_* y}{v}$ Where the nominator is the multiplication of the friction velocity, u sub star and y is distance to nearest wall the denominator is the local kinematic viscosity of the fluid. For an accurate prediction for the k-ω model, it was stated that, even for y+ values of between 2 and 100, the shear stress at the wall computed varies at less than 2% ,Menter, Kuntz and Langtry [11]. Figure 4 gives the reported average y+ value across the airfoil surface for the current simulation. The residual convergence graph Figure 5 shows how the iterative numerical calculations of the solver were reduced to within an extremely low error bar for each parameter (x- velocity, y-velocity, k, ω and continuity).

It can be seen from Figure 5 that a highly accurate error bar of at least 1e-06 was achieved, meaning that calculated values are correct to within this limit (x and y velocities converged at around 1e-08, k and ω residuals converged in the region of 1e-12). Note how there are three sections to the graph; each represents a solver 'order'; initial simulation was done at first order, then second, then finally a third order solution was produced, to increase the precision of results.

5.2 Data & Results

Several results have been obtained relating to noise mechanisms across the NACA 0012 airfoil at 20m/s; these are pressure coefficient, turbulent intensity (%), surface acoustic power level (dB), self-noise and shear noise from x directional sources, and self-noise and shear noise from y directional sources (units are m/s^2) this is illustrated in figures 6, 7, 8 and 9.

Note that an individual validation section is unnecessary for this CFD simulation, since the method of ensuring a quality mesh and simulation environment has been described in the previous section. However, the similarity between the coefficient of pressure graphs for 0° in the present simulation and against the 3-D simulation of a much similar NACA 0012 airfoil (and Reynolds number) at 0° by Marsden, Bogey and Bailly [12] is clear – values are very similar with insignificant deviation, proving that the simulation which has been performed has achieved valid results. Results compiled will henceforth be discussed.

6.1 CFD Simulation

The inclusion of CFD further supports the claims made in the previous section on the summary of the experimental data. When the simulated pressure distributions (represented by contours in figure 6 and graphs in figure 9) are observed, it can be surmised that the adverse pressure gradients do in fact steepen, as expected, with angle of attack, in figure 9 the upper surface is represented by the bottom curve, and the lower surface by the top curve (upper surface is negative, lower surface is positive).

When reviewing the turbulence intensity contours and graphs (figures 8 and 9) against the contours and graphs of surface acoustic power level (figures 10 and 11), it is clear that there is an almost direct correlation between the energy contributed by turbulent structures (i.e. vortices), and the level of noise measured at the surface, and within the boundary layer of the airfoil. In the case of each of these graphs, the upper surface is represented by the curve which has a high peak at the location of the leading edge, which, as angle of attack is increased, trails off towards the trailing edge until some point at which the turbulence intensity (and hence surface acoustic power level) of the lower surface is higher. As suggested in the previous discussion on the physical acoustic testing, as the adverse pressure gradient along the upper surface boundary layer becomes stronger with angle of attack, vortices near to the surface of the trailing edge associated with turbulence cease as the boundary layer begins to separate, and this is reflected in the plots of vorticity (figure 12) for each angle of attack. Of course, since the adverse pressure gradient of the lower surface *straightens out* with angle of attack, the boundary layer remains attached, and vorticity becomes stronger due to downstream turbulence.

Also, looking at the upper surface chord location x point of around 0.03m for both the turbulence intensity and surface acoustic power level graphs at 16° angle of attack, a distinct trough can be seen, which, when looking closely at this point on the contour plots of figure 7(c) and 10(c), can be seen to be due to a small scale separation bubble, which then reattaches again to become part of the turbulent boundary layer.

A final discernment can be gained by viewing the x and y-directional self-noise and shear-noise source plots of figures 13 to 18; generally as angle of attack is increased both x and y sources have the same trends, yet, y sources (perpendicular to the free-stream flow) appear to have a bigger impact as angle of attack is increased. This solidifies the assumption made in the previous reported study [9] , and can be explained by the propagation of Tollmien-Schlichting waves, which of course increase in amplitude (a y directional source), along the airfoil. Also, as the angle of attack is increased, x sources (viscous and shear effects) appear to have less of an effect with increase in angle of attack. These observations clearly show that as angle of attack is increased, shear noise contributes less and less energy further downstream of the airfoil, and becomes dominated by noise energy from vortical structures within turbulence, such as Kelvin-Helmholtz instabilities.

As for potential sources of error in the CFD simulation section describes the methodology by which an accurate simulation environment has been created; the validation source in figure 62 shows that the simulation has been performed with high accuracy.

4. Conclusions

Airfoil self-noise or trailing edge noise and shear noise was investigated computationally for a NACA0012 airfoil section, focusing on noise mechanisms at the trailing edge to identify and understand sources of noise production using ANSYS Fluent. A two-dimensional computational fluid dynamics simulation has been performed for 0°, 8° and 16° airfoil angle of attack capturing surface pressure contours, contours of turbulent intensity, contours of surface acoustic power

level, vorticity magnitude levels across the airfoil profile, and x and y directional self and shear noise sources across the airfoil profile. The results, indicate that pressure gradients at the upper surface do increase as the angle of attack increase which is a measure of vortices near the surface of the trailing edge associated with turbulence cease as the boundary layer begins to separate. Comparison of the turbulent intensity contours with surface acoustic power level contours demonstrated direct correlation between the energy contributed by turbulent structures (i.e. vortices), and the level of noise measured at the surface, and within the boundary layer of the airfoil. As angle of attack is increased both x and y sources have the same trends, yet, y sources (perpendicular to the free-stream flow) appear to have a bigger impact as angle of attack is increased. Furthermore, as the angle of attack increased, shear noise contributes less and less energy further downstream of the airfoil, and becomes dominated by noise energy from vortical structures within turbulence. The two-dimensional computational fluid dynamics simulation revealed pressure, turbulent intensity and surface acoustic power contours, that further corroborated the previously tested noise observations phenomena reported by the authors at the trailing edge of the airfoil.

Acknowledgments

The research was conducted by Beren R Jackson in partial fulfillment of BSc (Hons) in Aerospace Technology at the Department of Engineering and Math at Sheffield Hallam University under the supervision of Dr. Sam M Dakka.

References

[1] Brooks, T.F., Pope, D.S. and Marcolini, M.A., "Airfoil Self-Noise and Prediction," Technical Report. NASA Reference Publication 1218, 1989, pp. 1-146

[2] Roger, M. and Moreau, S., "Broadband self-noise from loaded fan blades," AIAA Journal, Vol. 42, No. 3, 2004, pp. 536-544

[3] Roger, M., Moreau, S., "Trailing Edge Noise Measurements and Prediction for Subsonic Loaded Fan Blades, AIAA Paper No. 2002-2460," 8th AIAA/CEAS Aeroacoustics Conference & Exhibit, Breckenridge, Colorado, 17-19 June 2002.

[4] FfowcsWilliams, J. and Hall, L., "Aerodynamic sound generation by turbulent flow in the vicinity of a scattering half-plane," Journal of Fluid Mechanics, Vol. 40, 1970, pp. 657–670.

[5] Amiet, R., "Noise due to turbulent flow past a trailing edge," Journal of Sound and Vibration Vol. 47, 1976, pp. 387–393.

[6] Howe, M., "A review of the theory of trailing edge noise," Journal of Sound and Vibration Vol. 61, 1978, pp. 437–465.

[7] Brooks, T.F., Pope, D.S. and Marcolini, M.A., "Airfoil Self-Noise and Prediction," Technical Report. NASA Reference Publication 1218, 1989, pp. 1-146

[8] Brooks, T.F. and Hodgson, T.H., "Trailing edge noise prediction from measured surface pressures," Journal of Sound and Vibration, Vol. 78, 1981, pp. 69–117

[9] Jackson, B.R. and Dakka, S.M., "An Investigation into Flow Behavior and Acoustic Mechanisms at the Trailing Edge of an Airfoil," Journal of Noise and Vibration Worldwide, Vol. xx, 2016, pp. xx-xx

[10] Bardina, J.E., Huang, P.G. and Coakley, T.J., "*Turbulence Modeling Validation, Testing, and Development*," California: NASA, Available: http://www.ewp.rpi.edu/hartford/~ferraj7/ET/Other/References/nasa_techmemo_110446.pdf.

[11] Menter, F.R., Kuntz, M. and Langtry, R., "*Ten Years of Industrial Experience with the SST Turbulence Model*," Otterfing, Germany, 2003: ANSYS-CFX.

[12] Marsden, O., Bogey, C. and Bailly, C., "*Direct Noise Computation around a 3-D NACA 0012 airfoil*," Massachusetts: AIAA, 2006-2503

FIGURE CAPTIONS

Figure 1. Generated mesh for 2D CFD simulation.

Figure 2. Close-up of airfoil and mesh.

Figure 3. Mesh cell orthogonal quality (left) and mesh cell skewness (right).

Figure 4. Reported average y+ value for NACA 0012 2-D CFD simulation.

Figure 5. Solver residuals convergence graph against iterations.

Figure 6. Contours of pressure coefficient for (a) 0°, (b) 8° and (c) 16° angle of attack.

Figure 7. Contours of turbulent intensity for (a) 0°, (b) 8° and (c) 16° angle of attack

Figure 8. Graphs of turbulent intensity across the airfoil profile for 0° (top-left), 8° (top-right) and 16° (bottom).

Figure. 9. Graphs of pressure coefficient across the airfoil profile for 0° (top-left), 8° (top-right) and 16° (bottom-left). A validation source is also included for comparison with 0° (bottom-right), (Marsden, Bogey and Bailly, 2006).

Figure 10. Contours of surface acoustic power level (dB) for (a) 0°, (b) 8° and (c) 16° angle of attack.

Figure .11. Graphs of surface acoustic power level (dB) across the airfoil profile for 0° (top-left), 8° (top-right) and 16° (bottom).

Figure 12. Graphs of vorticity magnitude (1/s) across the airfoil profile for 0° (top-left), 8° (top- right) and 16° (bottom).

Figure 13. Graphs of x-directional noise sources (m/s^2) across the airfoil profile for 0°, self-noise (left) and shear noise (right).

Figure 14. Graphs of x-directional noise sources (m/s^2) across the airfoil profile for 8°, self-

List of Tables

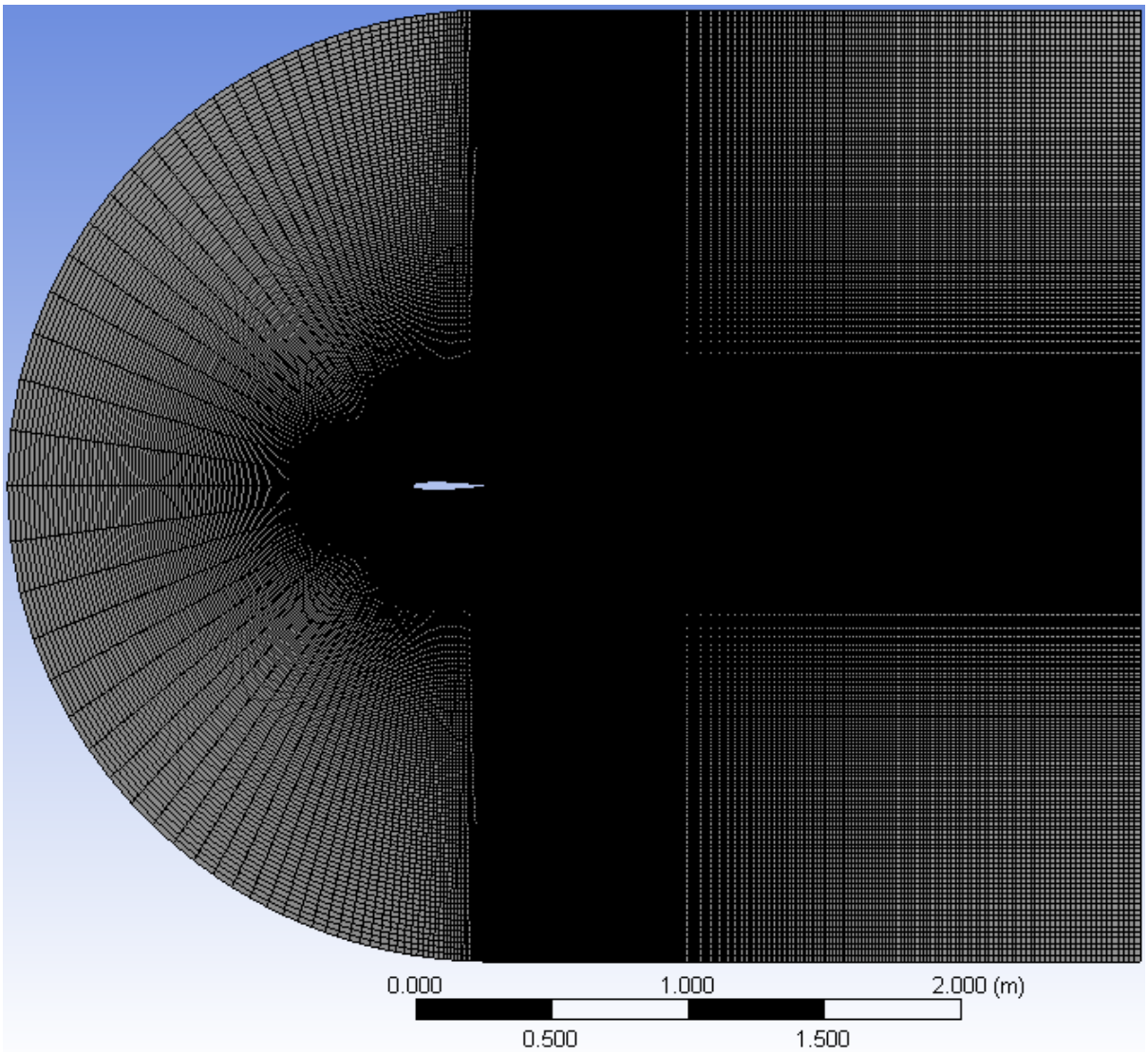

Fig. 1. Generated mesh for 2D CFD simulation.

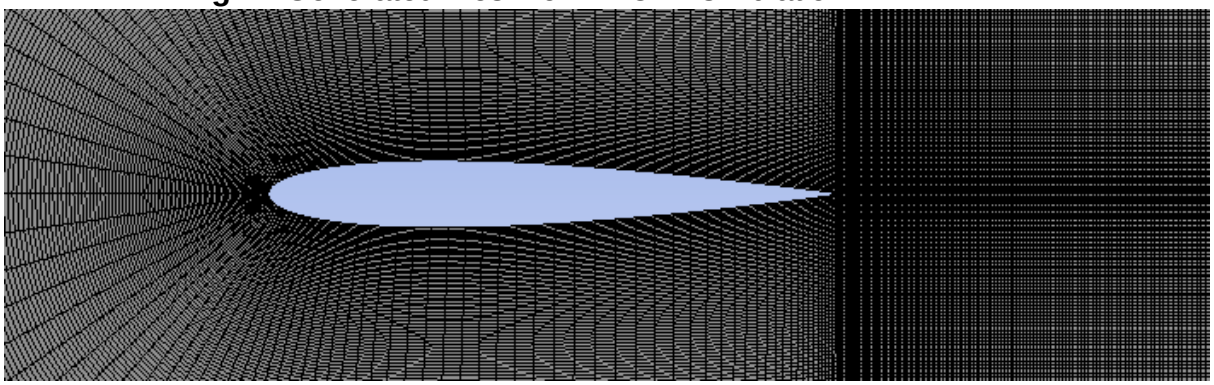

Fig. 2. Close-up of airfoil and mesh.

56

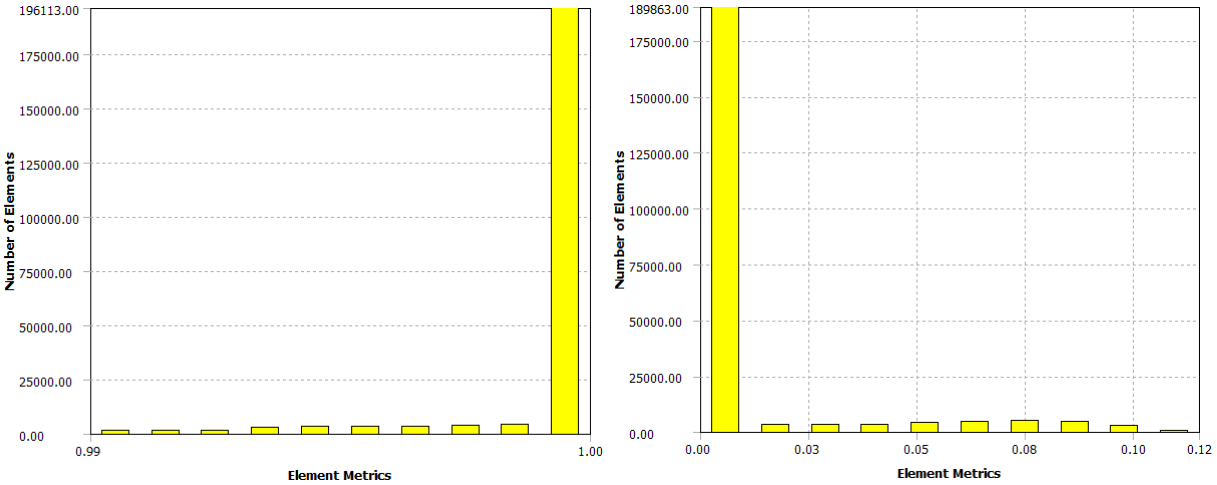

Fig. 3. Mesh cell orthogonal quality (left) and mesh cell skewness (right).

```
Average of Facet Values
                  Wall Yplus
------------------------- --------------------

                  airfoil                36.656101
```

Fig. 4. Reported average y+ value for NACA 0012 2-D CFD simulation.

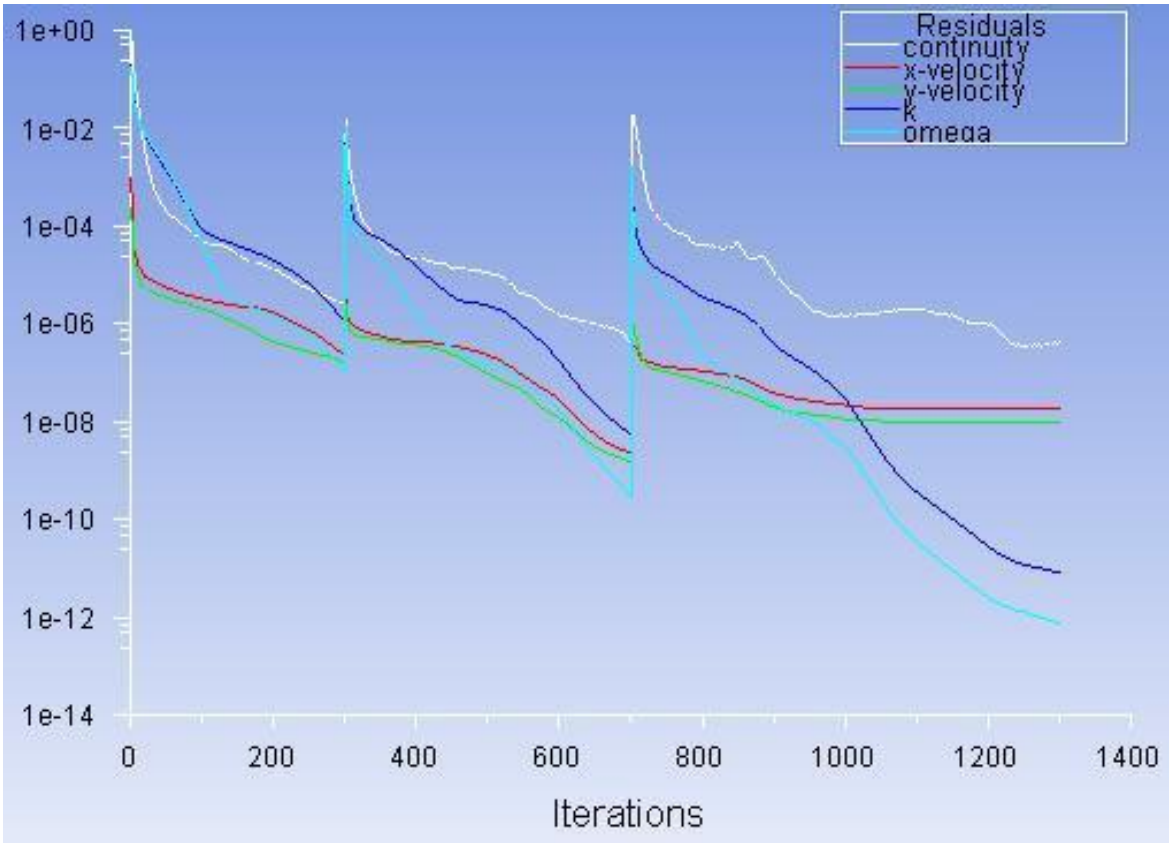

Fig. 5. Solver residuals convergence graph against iterations.

(a)

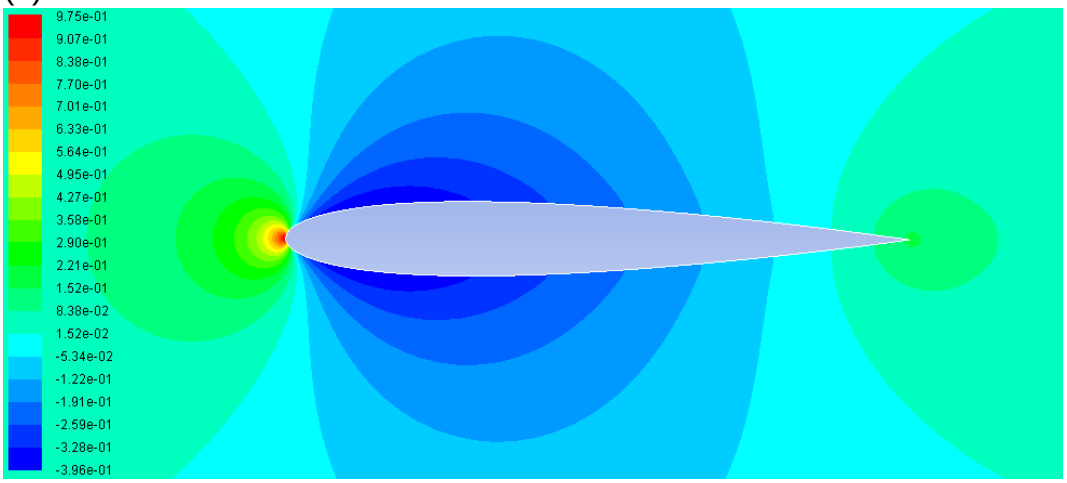

(b)

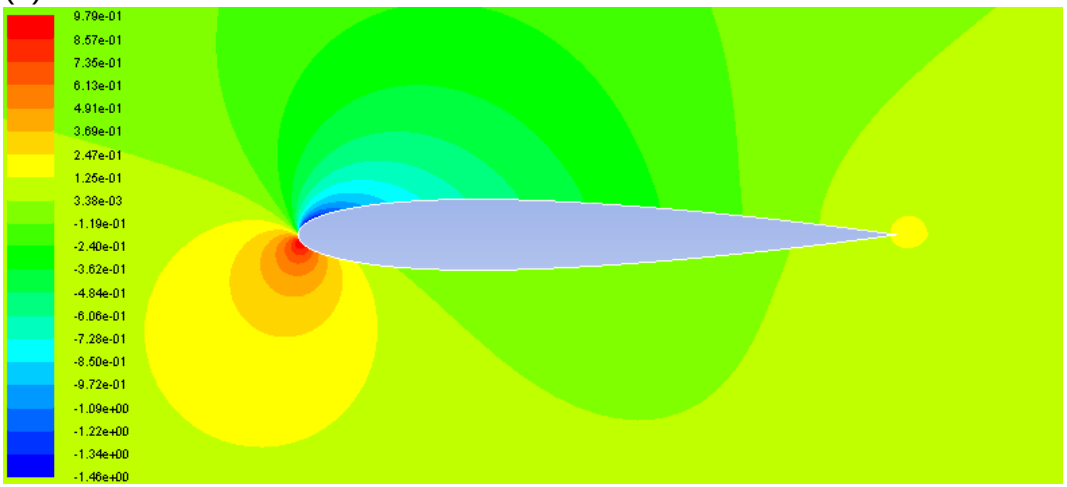

(c)

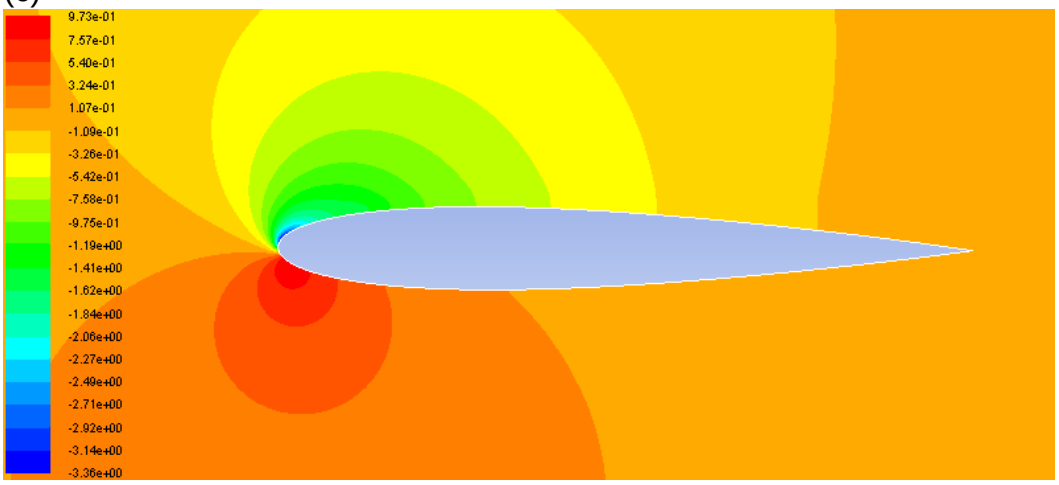

Fig. 6. Contours of pressure coefficient for (a) 0°, (b) 8° and (c) 16° angle of attack.

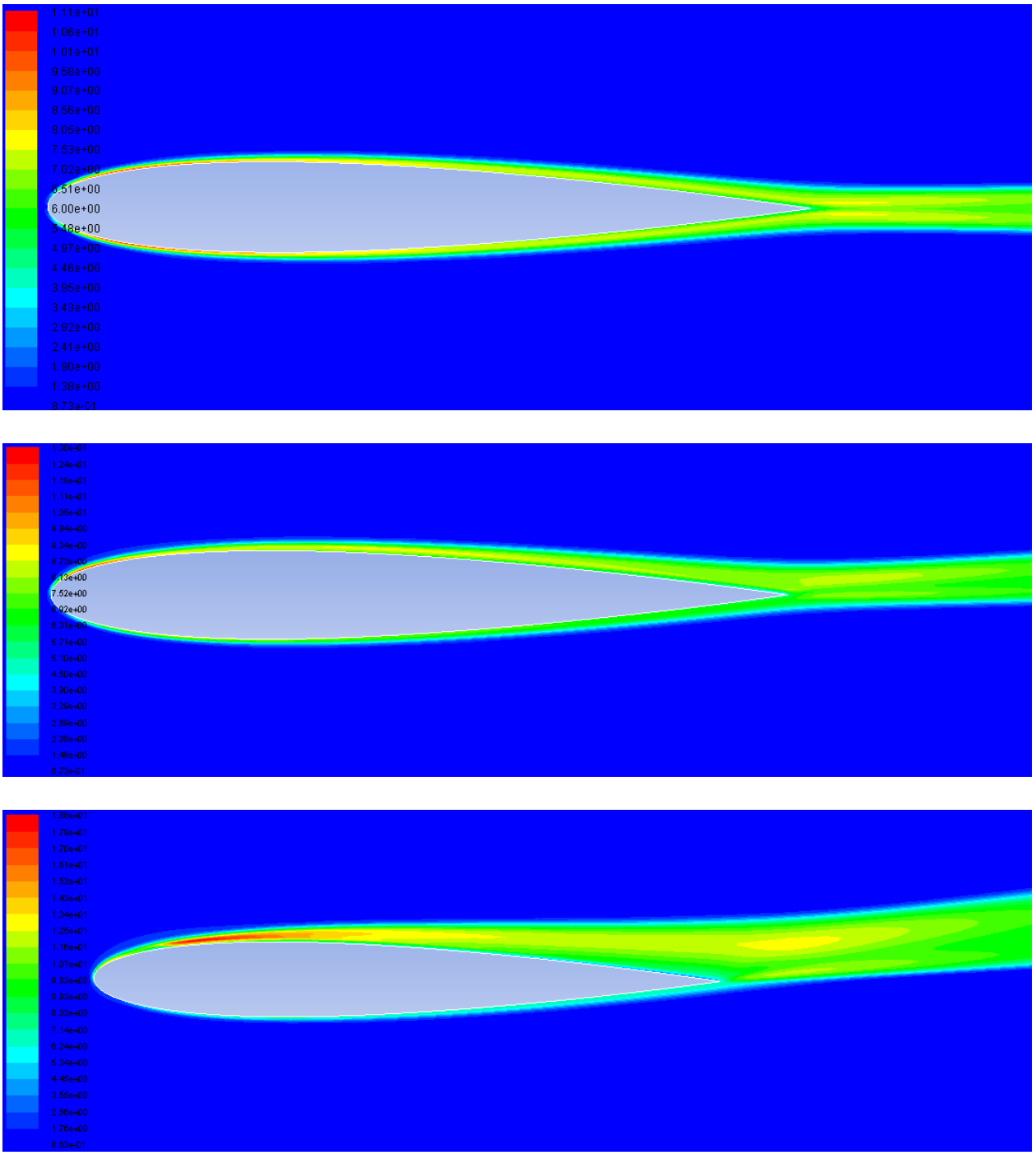

Fig. 7. Contours of turbulent intensity for (a) 0°, (b) 8° and (c) 16° angle of attack

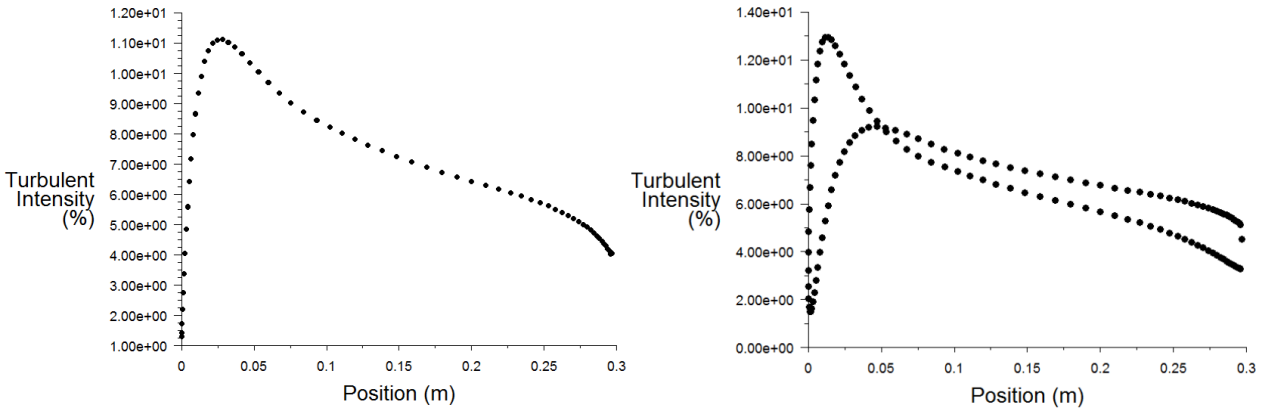

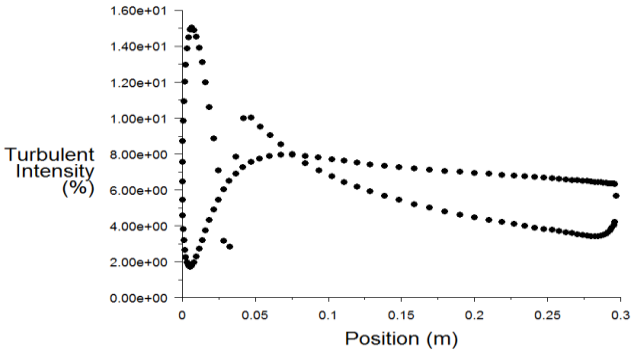

Fig. 8. Graphs of turbulent intensity across the airfoil profile for 0° (top-left), 8° (top-right) and 16° (bottom).

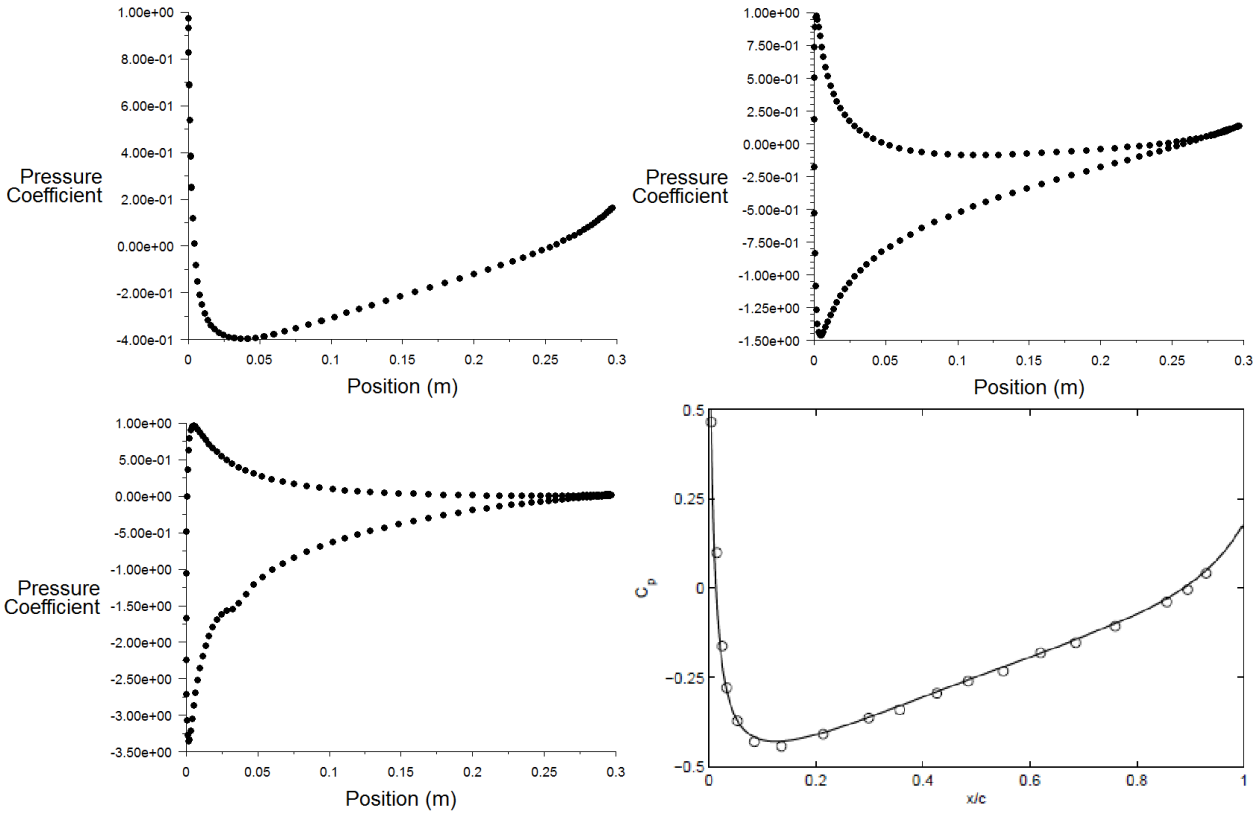

Fig. 9. Graphs of pressure coefficient across the airfoil profile for 0° (top-left), 8° (top-right) and 16° (bottom-left). A validation source is also included for comparison with 0° (bottom- right), (Marsden, Bogey and Bailly, 2006).

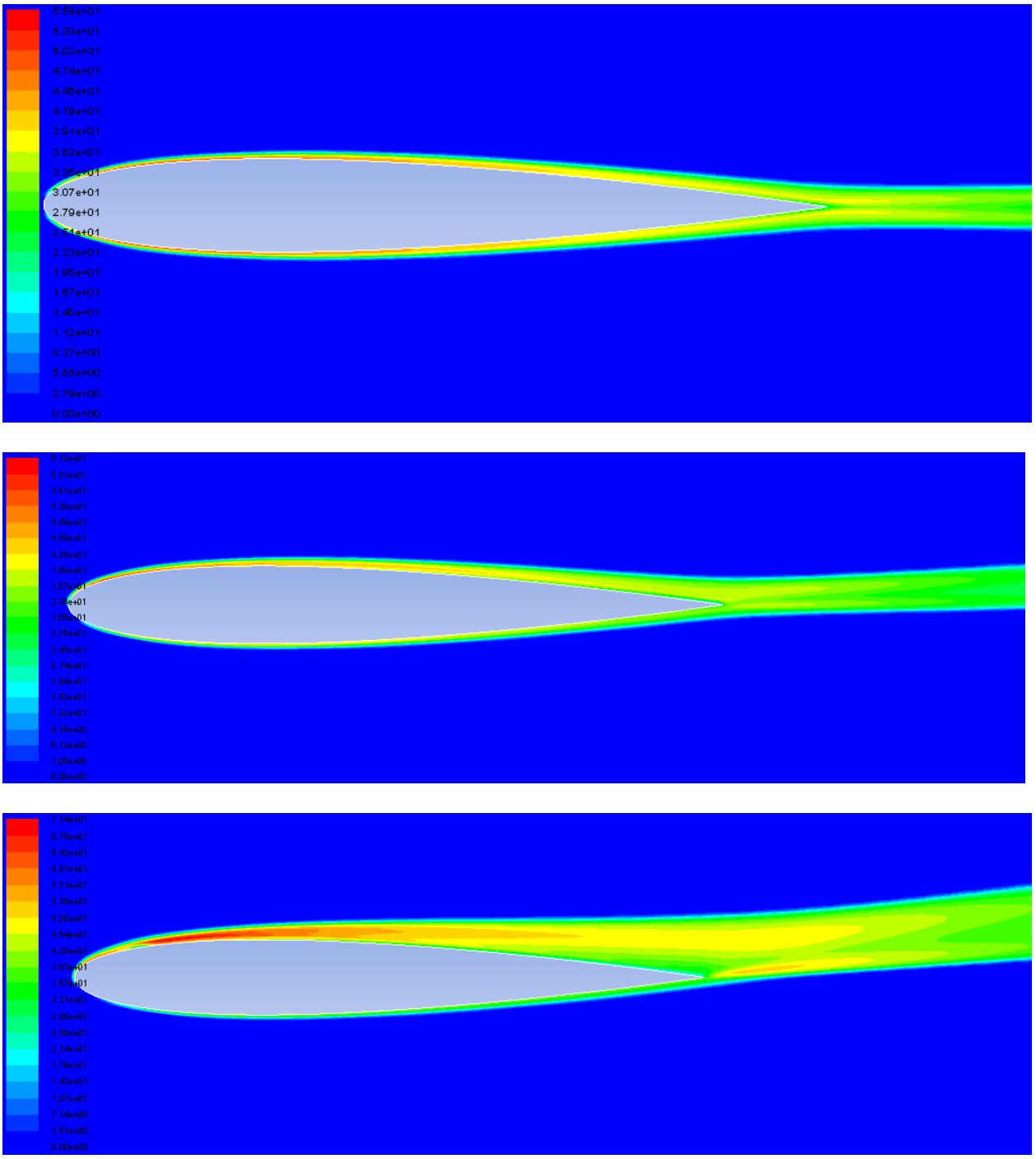

Fig. 10. Contours of surface acoustic power level (dB) for (a) 0°, (b) 8° and (c) 16° angle of attack.

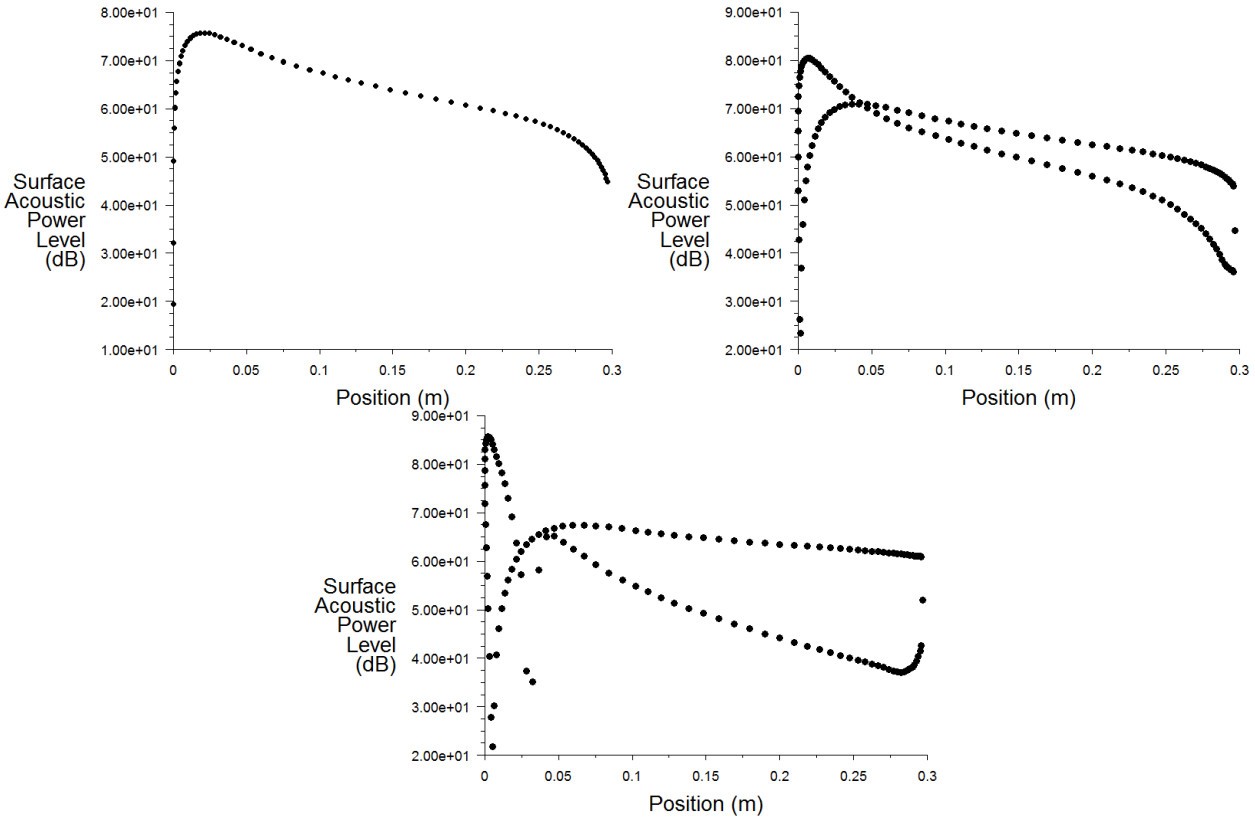

Fig. 11. Graphs of surface acoustic power level (dB) across the airfoil profile for 0° (top- left), 8° (top-right) and 16° (bottom).

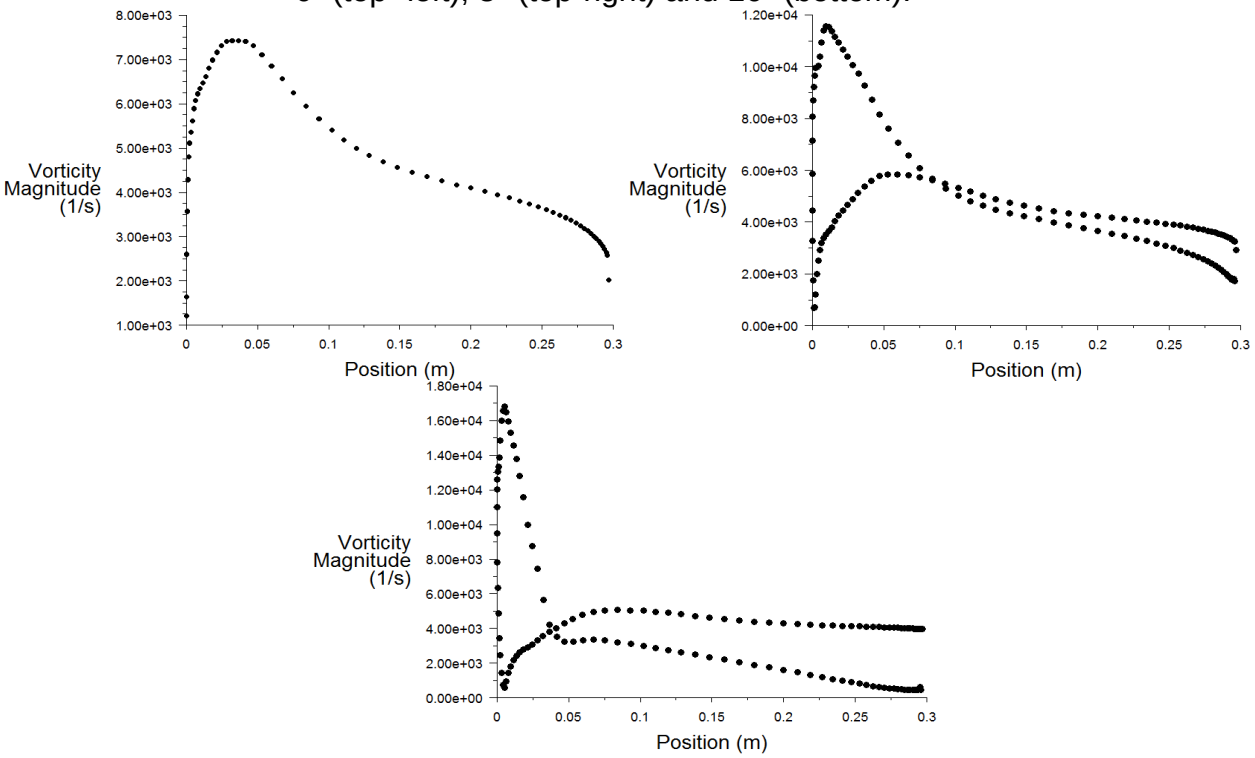

Fig.12. Graphs of vorticity magnitude (1/s) across the airfoil profile for 0° (top-left), 8° (top- right) and 16° (bottom).

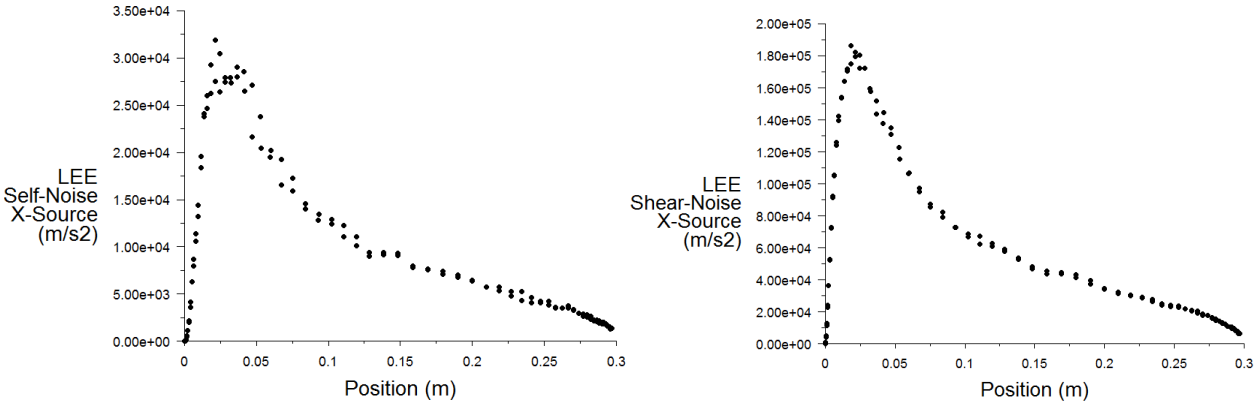

Fig.13. Graphs of x-directional noise sources (m/s^2) across the airfoil profile for 0°, self- noise (left) and shear noise (right).

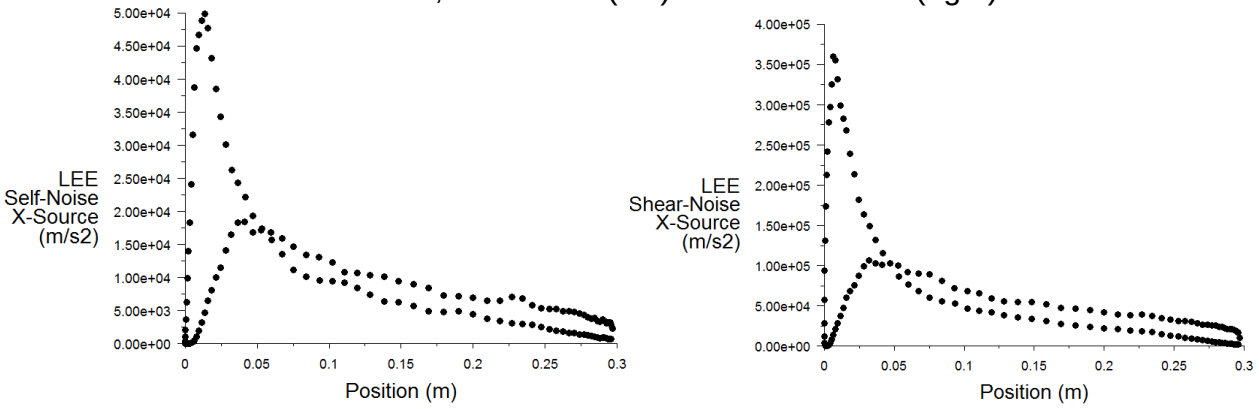

Fig.14. Graphs of x-directional noise sources (m/s^2) across the airfoil profile for 8°, self- noise (left) and shear noise (right).

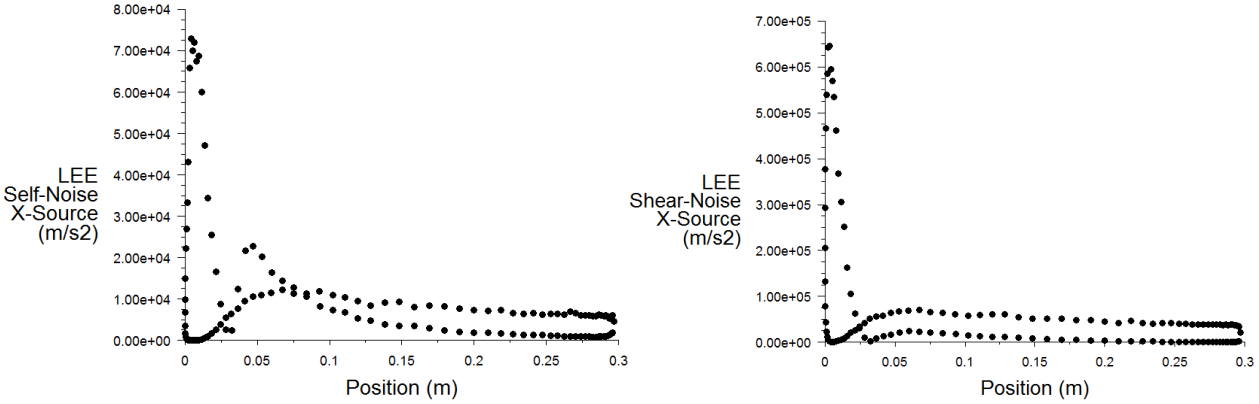

Fig.15. Graphs of x-directional noise sources (m/s^2) across the airfoil profile for 16°, self- noise (left) and shear noise (right).

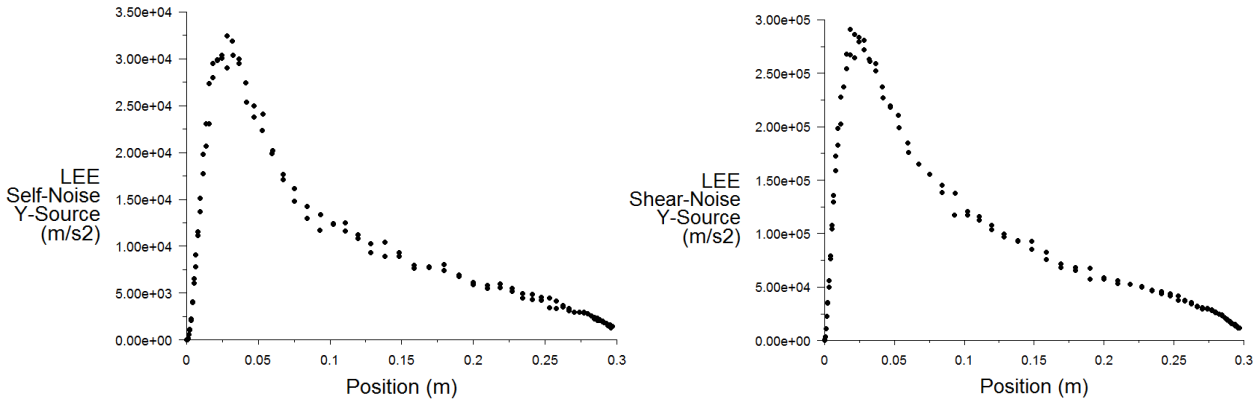

Fig.16. Graphs of y-directional noise sources (m/s^2) across the airfoil profile for 0°, self- noise (left) and shear noise (right).

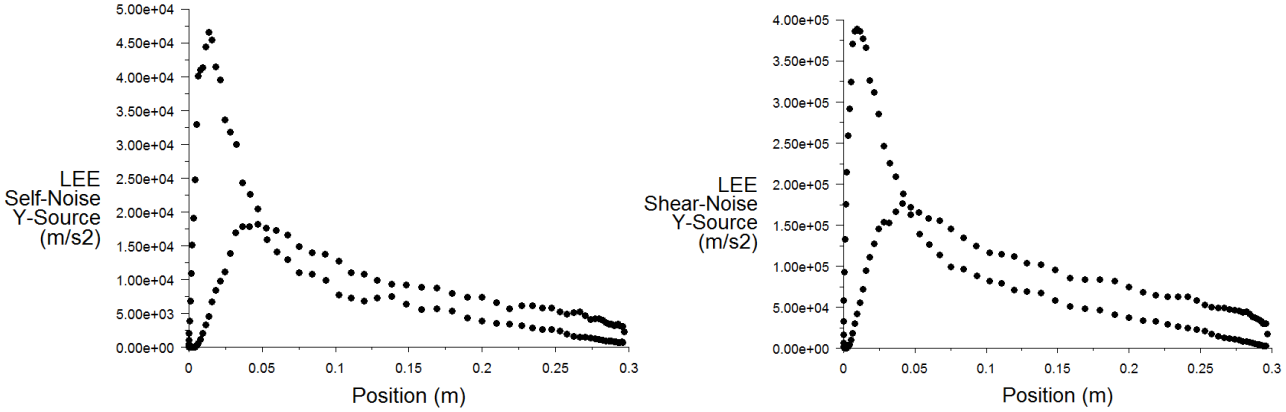

Fig.17. Graphs of y-directional noise sources (m/s^2) across the airfoil profile for 8°, self- noise (left) and shear noise (right).

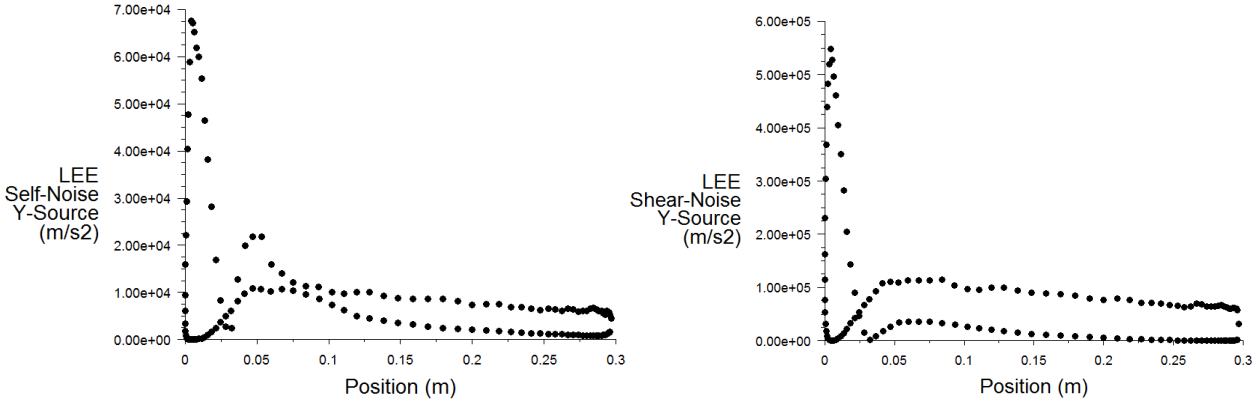

Fig. 18. Graphs of y-directional noise sources (m/s^2) across the airfoil profile for 16°, self- noise (left) and shear noise (right).

Table 1: Positions of each microphone in relation to airfoil chord length

Microphone No.	X/C	Distance from Leading Edge/mm	Distance from mid-span/mm
1	0.613	182	0
2	0.646	192	0
3	0.680	202	0
4	0.714	212	0
5	0.747	222	0
6	0.781	232	0
7	0.815	242	0
8	0.848	252	0
9	0.882	262	0
10	0.916	272	0

Table 2: Element metric values:

-	Orthogonal Quality	Skewness
Minimum	0.986	1.3×10^{-10}
Maximum	1	0.115
Average	0.999	8.37×10^{-3}